Editors' Suggestion

Room temperature magnetic vortices in the van der Waals magnet Fe_5GeTe_2

Elias Sfeir,[1] Carolin Schrader,[1] Florentin Fabre,[1] Jules Courtin,[2] Céline Vergnaud,[2] Alain Marty,[2] Matthieu Jamet,[2] Frédéric Bonell,[2] Isabelle Robert-Philip,[1] Vincent Jacques,[1] and Aurore Finco[1,*]

[1]*Laboratoire Charles Coulomb, Université de Montpellier, CNRS, Montpellier, France*

[2]*Université Grenoble Alpes, CNRS, CEA, SPINTEC, 38054 Grenoble, France*

(Received 4 July 2025; accepted 27 October 2025; published 21 November 2025)

We investigate the effect of confinement on the magnetic state of a 12-nm-thick Fe_5GeTe_2 layer grown by molecular beam epitaxy. We use quantitative scanning nitrogen-vacancy magnetometry to locally extract the magnetization in rectangular uniformly in-plane magnetized microstructures, showing no enhancement of the Curie temperature compared to magnetization measurements performed before patterning the film, in contrast to previous results obtained on thick Fe_3GeTe_2 flakes. Under the application of a weak out-of-plane magnetic field, we observe the stabilization of magnetic vortices at room temperature in micrometric squares. Finally, we highlight the effect of the size of the patterned microdisks and microsquares on the stabilization of the vortices using experiments and micromagnetic simulations. Our work thus proposes and demonstrates a way to stabilize noncollinear textures at room temperature in a van der Waals magnet using confinement.

DOI: 10.1103/v5zf-5z78

I. INTRODUCTION

Among the broad diversity of van der Waals magnets discovered in recent years, very few possess a Curie temperature T_C above room temperature [1], which is a crucial requirement for technological applications. In particular, Fe_5GeTe_2 possesses a T_C of about 300 K in bulk [2–4], which remains high (>200 K) in few-layers-thick films or flakes [2,5–8]. It was also shown that its Curie temperature can be significantly enhanced above room temperature by substituting Fe with Co [9] or Ni [10]. This material is particularly interesting, as several groups have reported the observation or the prediction of magnetic bubbles, merons, and skyrmions [11–18], with discussions about the possible presence of a sizable bulk Dzyaloshinkii-Moriya interaction (DMI) [19,20] and about the role of oxidation in their stabilization [21,22]. The magnetic anisotropy in Fe_5GeTe_2 flakes has also been found to significantly vary [23]. Therefore, the nucleation and stabilization of these complex magnetic textures remains only partially controlled.

A solution could be to take advantage of dipolar energy and use confinement in order to stabilize whirling textures in micromagnetic structures. The effect of such patterning on Fe_5GeTe_2 has not been studied yet, but on the parent compound Fe_3GeTe_2, surprising effects have been observed. Li *et al.* [24] have reported X-ray magnetic circular dichroism and photoelectron emission microscopy experiments showing the presence of a spin reorientation transition from out of plane to in plane at 230 K in patterned Fe_3GeTe_2 flakes, together with a dramatic increase of T_C above room temperature. The resulting microstructures thus exhibit a vortex state at 300 K. As pointed out by Li *et al.*, it remains unclear whether this strong variation of magnetic properties originates from size effects or from a chemical alteration of the material during microfabrication. Here, we investigate the influence of patterning on the magnetic state of a Fe_5GeTe_2 thin film grown by molecular beam epitaxy (MBE) [7], which is thus already ferromagnetic at room temperature. In particular, we study the effect of confinement on the stabilization of noncollinear magnetic textures such as vortices. In order to perform this analysis and to obtain local information about T_C by extracting the value of the magnetization in different microstructures, we use scanning nitrogen-vacancy (NV) center magnetometry [25]. This technique allows us to map quantitatively the magnetic stray field produced by the Fe_5GeTe_2 microstructures, nonperturbatively and under ambient conditions. All the measurements presented in this work have been performed with a commercial scanning NV center microscope (ProteusQ, Qnami).

II. METHODS

Figure 1(a) presents a sketch of the experiment. Our sample is a 11.8-nm-thick Fe_5GeTe_2 film grown by MBE on $Al_2O_3(0001)$ by coevaporation of Fe, Ge, and Te with a flux ratio Fe:Ge = 5 and a slight excess of Te. The substrate temperature was 450 °C, as measured with a thermocouple located close to the sample holder. The growth was performed at a rate of 1 monolayer per minute, followed by annealing under Te flux up to 580 °C for 5 min. The sample was then cooled down to room temperature at a rate of 5–10 K min^{-1}, then capped with a protective 3-nm-thick Al layer that naturally oxidized in air [7]. The film has been subsequently patterned with electron beam lithography and Ar ion etching in order to create microstructures of various sizes and shapes (squares, rectangles, and disks). Macroscopic characterization of a typical MBE-grown film of the same thickness before patterning using Superconducting Quantum Interference Device (SQUID) magnetometry is presented in

*Contact author: aurore.finco@umontpellier.fr

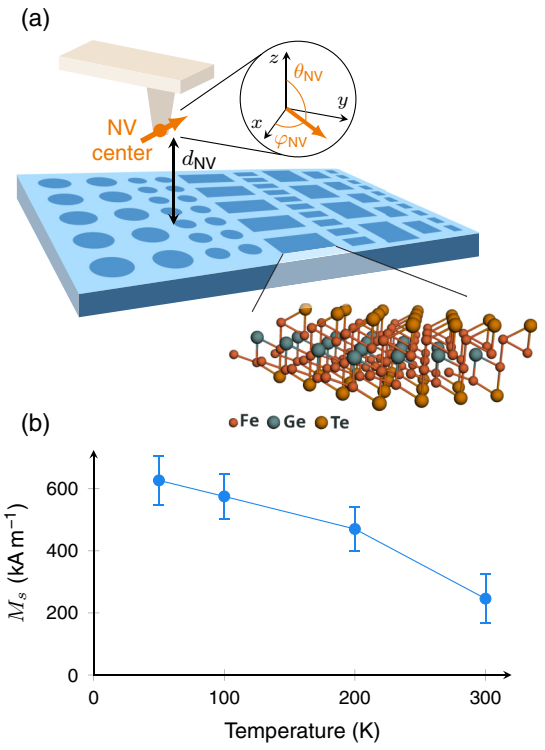

FIG. 1. (a) Sketch of the experiment. We use a diamond scanning probe to perform NV magnetometry experiments on a microstructured Fe_5GeTe_2 film. The top inset defines the angles θ_{NV} and φ_{NV} which describe the orientation of the NV center in the laboratory frame. The bottom inset displays the structure of a monolayer of Fe_5GeTe_2, drawn using the pyXtal library [26] and a cif file from the Computational 2D Materials Database [27,28]. (b) Typical SQUID measurement of M_s in a 12-nm-thick MBE grown film, indicating a Curie temperature above 300 K before patterning.

Fig. 1(b) and indicates that the film is magnetized in plane and exhibits a Curie temperature slightly above room temperature, with a saturation magnetization $M_s = 246 \pm 80$ kA m^{-1} at 300 K. A temperature-dependent magneto-optical Kerr effect measurement performed on the patterned sample before microfabrication is shown in the Supplemental Material [29] and confirms that the film is ferromagnetic at 300 K.

III. RESULTS

In a first series of measurements presented in Fig. 2, we perform scanning NV center magnetometry on microstructures of different sizes. The sample was initially in a demagnetized state since the microfabrication process involved an annealing above T_C. We use a permanent magnet to apply a tilted external magnetic field of 5.4 mT roughly aligned with the quantization axis of the NV center, which is described by the angles $\theta_{NV} \simeq 125^\circ$ and $\varphi_{NV} \simeq 87^\circ$ defined in Fig. 1(a). The field is sufficient to obtain rectangular microstructures hosting a single uniform magnetic domain, and its out-of-plane component is low enough to avoid tilting the magnetization $\vec{M}$ out of the *ab* plane. In this case, we expect to detect magnetic stray field at the edges orthogonal to $\vec{M}$, and no field at the edges parallel to $\vec{M}$. This corresponds perfectly to the experimental data shown in Fig. 2 for four different rectangular microstructures.

Since our measurements are quantitative, we can compute the saturation magnetization M_s from each map, by fitting the stray field to its analytical expression. To achieve this, we first extract a stray field profile across the edges which produce stray field. The positions of these line profiles are indicated by the black lines on the images in Fig. 2. With scanning NV center magnetometry, we measure the component B_{NV} of the stray field, which is its projection along the quantization axis of the NV center and can therefore be written as

$$B_{NV} = \sin\theta_{NV}\cos\varphi_{NV}B_x + \sin\theta_{NV}\sin\varphi_{NV}B_y + \cos\theta_{NV}B_z. \quad (1)$$

The magnetic stray field produced at an edge parallel to the y axis and located at $x = x_0$, with $\vec{M}$ orthogonal to the edge and measured at a height d_{NV}, can be written as [29]

$$B_x(x) = \frac{\mu_0 M_s}{2\pi}\left[\arctan\left(\frac{d_{NV} - \frac{t}{2}}{x - x_0}\right) - \arctan\left(\frac{d_{NV} + \frac{t}{2}}{x - x_0}\right)\right],$$

$$B_y(x) = 0,$$

$$B_z(x) = \frac{\mu_0 M_s}{4\pi}\left\{\log\left[\left(d_{NV} - \frac{t}{2}\right)^2 + (x - x_0)^2\right] - \log\left[\left(d_{NV} + \frac{t}{2}\right)^2 + (x - x_0)^2\right]\right\}, \quad (2)$$

where t is the film thickness. We can fit the experimental line profiles to a combination of Eqs. (1) and (2), considering two opposite edges in each profile. Although the distance d_{NV} between the NV center and the surface as well as the angles θ_{NV} and φ_{NV} can be calibrated independently, we consider d_{NV} as a free parameter in the fits because of the presence of resist residues on the surface of the sample. These fits are plotted in the graphs at the bottom of Fig. 2, where the resulting value of M_s is also indicated. The main conclusion from this analysis is that M_s does not vary significantly with the size of the microstructure. However, we note that it seems that M_s decreases slightly when the area of the rectangle decreases, although the values do not deviate much from the error bars. This could be related to moderate damage made to the film during the patterning procedure. Since the average value that we obtain, $M_s = 202 \pm 12$ kA m^{-1}, is in good agreement with the value of M_s measured by SQUID at 300 K, we conclude that the microstructuring does not help increasing T_C in our experiment. In particular, we do not observe the strong enhancement reported in Ref. [24] for Fe_3GeTe_2. This suggests that these results were probably the consequence of a chemical alteration of Fe_5GeTe_2 by Ga implantation. It has indeed recently been shown that replacing Ge with Ga leads to an increase of T_C up to 350–380 K in Fe_3GeTe_2 [30] and Fe_5GeTe_2 [31] and to the observation of skyrmions in thick flakes of Fe_3GaTe_2 [32,33]. Theoretical investigations attribute this effect to higher-order exchange coefficients which are positive in Fe_3GaTe_2 in contrast to Fe_3GeTe_2 in which they are negative [34].

In a second series of measurements, we reduce the applied magnetic field to 3.6 mT out of plane. This field allows us to determine the sign of the measured magnetic field during

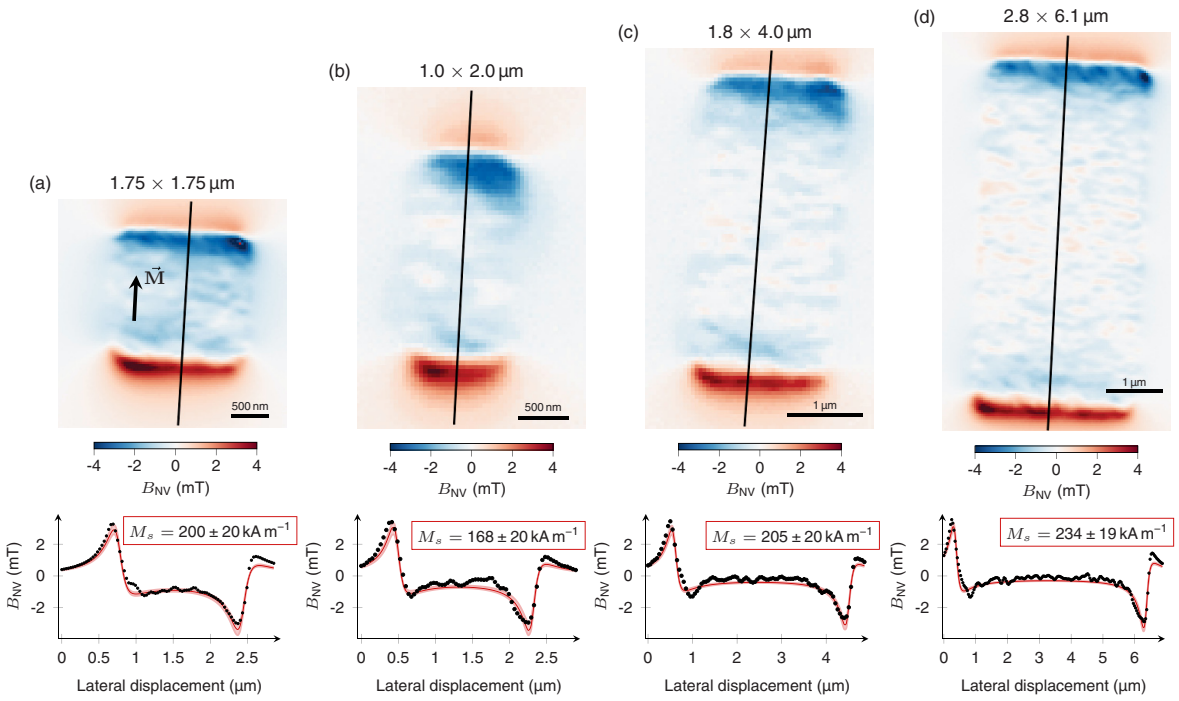

FIG. 2. Measurement of M_s in microstructures of different sizes. The maps show the measured stray magnetic field under a tilted external magnetic field of 5.4 mT, allowing us to stabilize a single domain in each rectangle. The plots below each map show the profiles extracted along the black lines and the corresponding fits with Eqs. (1) and (2), together with the extracted M_s value.

the NV magnetometry scans [35] and has a limited effect on the magnetic texture inside the Fe_5GeTe_2 microstructures. Similarly to what was observed in the images of the Fe_3GeTe_2 microstructures in Ref. [24], our magnetic stray field maps reveal the presence of magnetic vortices in some of the square structures [see Figs. 3(a) and 3(b)]. Indeed, we detect a flower-shaped stray field pattern, which is typical for vortices [36], in squares of different sizes and orientations with respect to the crystal structure of Fe_5GeTe_2.

However, as the vortex cores are not visible in our images, we performed additional micromagnetic simulations to really ensure that we are observing vortices. We used the Python package Ubermag [37] with OOMMF [38] to compute the relaxed magnetic configurations in the two squares considered in Fig. 3, and computed the associated magnetic stray field map at the NV center height using a scalar potential method

TABLE I. Parameters used in the micromagnetic simulations and the subsequent stray field calculations.

Parameter	Value
NV height d_{NV}	120 nm
NV polar angle θ_{NV}	125°
NV azimuthal angle φ_{NV}	87°
Exchange stiffness A	10 pJ m^{-1}
Uniaxial anisotropy K_u	−20 kJ m^{-3}
Film thickness t	11.8 nm
Saturation magnetization M_s	202 kA m^{-1}
M_s disorder, patch size	∼50 nm
M_s disorder, variation amplitude	± 20%

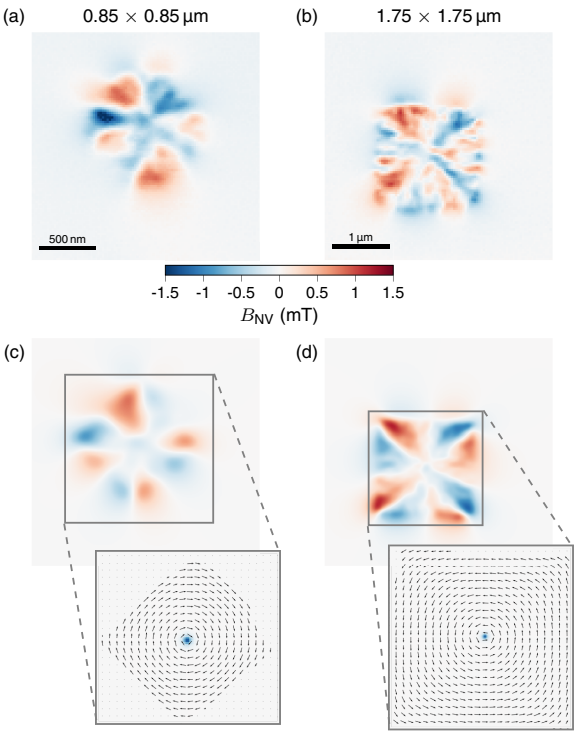

FIG. 3. (a), (b) Measured stray field maps of vortices in square microstructures. (c), (d) Computed stray field maps resulting from the magnetic state shown in the insets. The insets show the magnetization configurations obtained from micromagnetic calculations with the parameters from Table I, with the blue color indicating the core of the vortices where the magnetization tilts out of plane.

[39]. We write the magnetic field as the gradient of a scalar potential ϕ verifying the Poisson equation below [Eq. (3)], which we solve in Fourier space for computational efficiency.

$$\Delta\phi = \nabla \cdot \vec{M}. \tag{3}$$

We extracted the shape of the microstructures from the topography measurements, and used the parameters gathered in Table I. We chose a value for the exchange stiffness which corresponds to the order of magnitude given in the literature, 10 pJ m^{-1} [13,16,17]. Macroscopic measurements of the uniaxial anisotropy K_u shown in Fig. S3(a) [29] indicate that it is negative and vanishes around room temperature. Using the slightly positive value of 18 ± 30 kJ m^{-3} measured at 300 K results in the presence of a large and clearly visible vortex core in the center of the square microstructure (see Fig. S4), which does not match with our experiments. We have therefore varied K_u below this value in order to get images which are in better agreement with experimental data, and used $K_u = -20$ kJ m^{-3}. Using this value, the vortex core cannot be distinguished in the stray field images, in agreement with our measurements. In addition, although the presence of DMI has been demonstrated in our films [19], we do not include it in our simulation, as the effective in-plane anisotropy does not favor the stabilization of skyrmionic states. We also added some disorder in the simulations in order to mimic local variations of thickness or of M_s by defining random grains with a Voronoi tesselation and attributing them a random M_s value, with a variation of $\pm 20\%$ around the measured mean value $M_s = 202$ kA m^{-1}. Note that this M_s distribution is not directly related to the measurement uncertainty on the M_s value in Fig. 2, which provides an average value on the microstructure, but describes very local variations resulting from disorder and thickness fluctuations. Structural characterization of our films [7] indeed shows the presence of domains, a few tens of nm in size, epitaxially oriented but with a finite mosaic spread of $\sim 3^\circ$. Atomic steps are also present on the surface, indicating local thickness variations on the scale of our microstructures.

The NV-to-sample distance d_{NV} was assumed rather large, 120 nm, in agreement with the fits shown in Fig. 2 (see actual values in Supplemental Material [29]). As expected, this value is higher than the one measured in the calibration because of the resist residues. The NV orientation $\theta_{\mathrm{NV}}, \varphi_{\mathrm{NV}}$ was determined from the calibration measurement (Fig. S2 [29]). Using this K_u value and including disorder, we obtain stray field maps in qualitative good agreement with the experimental ones. We therefore conclude that we are actually observing vortices in square Fe_5GeTe_2 microstructures at room temperature.

We performed similar experiments in disk-shaped microstructures, and observed either magnetic single domains in very small disks (diameter below 500 nm), or complicated flower-shaped patterns most probably resulting from disorder (see Fig. S4 [29]). In the disks, in the absence of disorder, we only expect to measure stray field at the vortex core [40,41], and this field is very weak, whereas with disorder, a stray field pattern resulting exclusively from this disorder and masking the vortex core can be observed. As a consequence, our experimental data do not allow us to decide experimentally if vortices are present. Our simulations including disorder and a vortex in the center of the disks show nevertheless a reasonable agreement with the experimental data.

Our experimental investigation of microstructures of different sizes (500 nm, 1 μm, 2 μm) indicates that there is a higher probability to observe one or several vortices in the large structures than in the small ones. In particular, we found several disks of diameter below 500 nm without any vortex, such as the one shown in the left inset of Fig. 4, while the large rectangles such as the one shown in Fig. 2(d) can exhibit several vortices in a low out-of-plane field (see Supplemental Material [29]). We investigated this question further in squares and disks using micromagnetic simulations, without disorder and external magnetic field applied. We considered squares of various sizes, from 100 nm to 2 μm as well as disks with diameters ranging from 100 nm to 2 μm. As an initial state, we use a completely random orientation of the magnetization in each cell. We performed the simulation with 20 different random initial configurations for each size, and counted the number of realizations in which one or several vortices or antivortices are present at the end of the relaxation. Our results are gathered in Fig. 4. The same trend, in agreement with our experiments, is observed for the disks and the squares. In the very small structures of typical size 100 nm, we never find a vortex. When the size increases, the probability to observe a vortex increases, and for a size above 1.5 μm, we systematically end up with a complicated magnetic state consisting in several vortices and/or antivortices.

IV. DISCUSSION

This size effect has been studied previously experimentally, analytically and numerically [42–47] in disks and squares of soft ferromagnets. The critical disk radius separating the vortex state from a roughly uniformly in-plane magnetized state in microdisks depends on the exchange stiffness, the saturation magnetization, and on the aspect ratio of the disks. In particular, most of the analytical calculations [44] have been performed for disks with a thickness larger than the exchange length [48]:

$$l_{\mathrm{ex}} = \sqrt{\frac{2A}{\mu_0 M_s^2}}. \tag{4}$$

In our case, $l_{\mathrm{ex}} \simeq 20$ nm, and therefore our disks are significantly thinner than l_{ex}, meaning that a two-dimensional (2D) model is more relevant [46]. It appears that for very thin films, the critical radius allowing the stabilization of vortices in a disk becomes very large [47], in agreement with our results presented in Fig. 4. We also note that the diameter of the core of the vortices in our simulations, which we obtained by fitting a two-dimensional gaussian function to the simulated maps of M_z, lies between 60 and 55 nm, again much larger than l_{ex}. Comparing this large core size with the dimensions of our simulated disks and squares, it appears that, as shown in Fig. 4, the 100-nm structures are too small to allow for the proper stabilization of a vortex.

To conclude, using quantitative scanning NV center magnetometry, we demonstrated that microstructuring does not significantly affect the Curie temperature in MBE-grown Fe_5GeTe_2 ultrathin films. However, by comparing experimental data with micromagnetic simulations, we revealed the

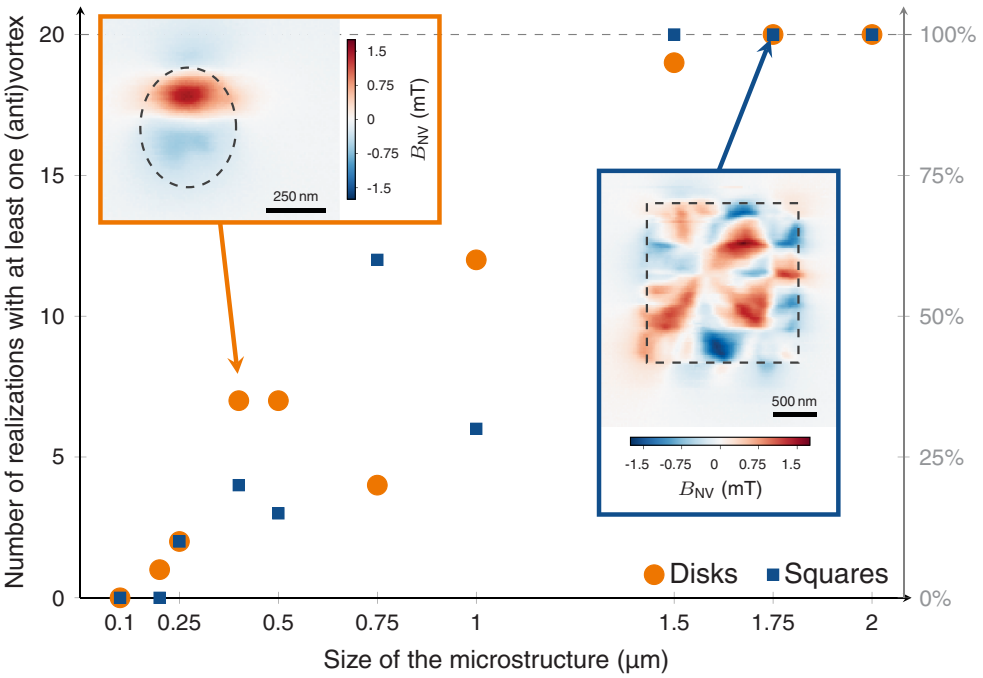

FIG. 4. Graph gathering the results of micromagnetic simulations of the magnetic state in disks and squares of various sizes, in the absence of external magnetic field and starting from random configurations. For each size and shape, 20 disorder configurations were considered. In the larger structures (>1.5 µm), several vortices and/or antivortices were systematically found. The insets show experimental data of a monodomain disk of diameter 0.4 µm and a multivortex square of size 1.75 µm, measured under a small out-of-plane magnetic field in order to bias the NV center.

presence of magnetic vortices in microstructures. We thus demonstrated here a way to control the formation of non-collinear magnetic textures at room temperature in Fe_5GeTe_2, opening perspectives to study the rich physics and potential applications of these objects in the context of 2D and van der Waals materials.

ACKNOWLEDGMENT

We acknowledge support from the French National Research Agency (ANR) via the project ELMAX (Grant No. ANR-20-CE24-0015), as well as through the program ESR/EQUIPEX+, with grant reference 2D-MAG (ANR-21-ESRE-0025) and through the France 2030 government investment plan under grant references PEPR SPIN – SPINMAT ANR-22-EXSP-0007 and PEPR SPIN – SPIN-CHARAC ANR-22-EXSP-0008.

DATA AVAILABILITY

The data that support the findings of this article are openly available [49].

[1] Q. H. Wang, A. Bedoya-Pinto, M. Blei, A. H. Dismukes, A. Hamo, S. Jenkins, M. Koperski, Y. Liu, Q.-C. Sun, E. J. Telford, H. H. Kim, M. Augustin, U. Vool, J.-X. Yin, L. H. Li, A. Falin, C. R. Dean, F. Casanova, R. F. L. Evans, M. Chshiev *et al.*, The magnetic genome of two-dimensional van der Waals materials, ACS Nano **16**, 6960 (2022).

[2] A. F. May, D. Ovchinnikov, Q. Zheng, R. Hermann, S. Calder, B. Huang, Z. Fei, Y. Liu, X. Xu, and M. A. McGuire, Ferromagnetism near room temperature in the cleavable van der Waals crystal Fe_5GeTe_2, ACS Nano **13**, 4436 (2019).

[3] A. F. May, C. A. Bridges, and M. A. McGuire, Physical properties and thermal stability of $Fe_{5-x}GeTe_2$ single crystals, Phys. Rev. Mater. **3**, 104401 (2019).

[4] J. Stahl, E. Shlaen, and D. Johrendt, The van der Waals ferromagnets $Fe_{5-\delta}GeTe_2$ and $Fe_{5-\delta-x}Ni_xGeTe_2$ – crystal structure, stacking faults, and magnetic properties, Z. Anorg. Allg. Chem. **644**, 1923 (2018).

[5] H. Chen, S. Asif, M. Whalen, J. Támara-Isaza, B. Luetke, Y. Wang, X. Wang, M. Ayako, S. Lamsal, A. F. May, M. A. McGuire, C. Chakraborty, J. Q. Xiao, and M. J. H. Ku, Revealing room temperature ferromagnetism in exfoliated Fe_5GeTe_2 flakes with quantum magnetic imaging, 2D Mater. **9**, 025017 (2022).

[6] Y. Deng, Z. Xiang, B. Lei, K. Zhu, H. Mu, W. Zhuo, X. Hua, M. Wang, Z. Wang, G. Wang, M. Tian, and X. Chen, Layer-number-dependent magnetism and anomalous Hall effect in van der Waals ferromagnet Fe_5GeTe_2, Nano Lett. **22**, 9839 (2022).

[7] M. Ribeiro, G. Gentile, A. Marty, D. Dosenovic, H. Okuno, C. Vergnaud, J.-F. Jacquot, D. Jalabert, D. Longo, P. Ohresser, A. Hallal, M. Chshiev, O. Boulle, F. Bonell, and M. Jamet,

Large-scale epitaxy of two-dimensional van der Waals room-temperature ferromagnet Fe_5GeTe_2, npj 2D Mater. Appl. **6**, 10 (2022).

[8] R. Fujita, P. Bassirian, Z. Li, Y. Guo, M. A. Mawass, F. Kronast, G. van der Laan, and T. Hesjedal, Layer-dependent magnetic domains in atomically thin Fe_5GeTe_2, ACS Nano **16**, 10545 (2022).

[9] A. F. May, M.-H. Du, V. R. Cooper, and M. A. McGuire, Tuning magnetic order in the van der Waals metal Fe_5GeTe_2 by cobalt substitution, Phys. Rev. Mater. **4**, 074008 (2020).

[10] X. Chen, Y.-T. Shao, R. Chen, S. Susarla, T. Hogan, Y. He, H. Zhang, S. Wang, J. Yao, P. Ercius, D. A. Muller, R. Ramesh, and R. J. Birgeneau, Pervasive beyond room-temperature ferromagnetism in a doped van der Waals magnet, Phys. Rev. Lett. **128**, 217203 (2022).

[11] Y. Gao, Q. Yin, Q. Wang, Z. Li, J. Cai, T. Zhao, H. Lei, S. Wang, Y. Zhang, and B. Shen, Spontaneous (anti)meron chains in the domain walls of van der Waals ferromagnetic $Fe_{5-x}GeTe_2$, Adv. Mater. **32**, 2005228 (2020).

[12] Y. Gao, S. Yan, Q. Yin, H. Huang, Z. Li, Z. Zhu, J. Cai, B. Shen, H. Lei, Y. Zhang, and S. Wang, Manipulation of topological spin configuration via tailoring thickness in van der Waals ferromagnetic $Fe_{5-x}GeTe_2$, Phys. Rev. B **105**, 014426 (2022).

[13] M. Schmitt, T. Denneulin, A. Kovács, T. G. Saunderson, P. Rüßmann, A. Shahee, T. Scholz, A. H. Tavabi, M. Gradhand, P. Mavropoulos, B. V. Lotsch, R. E. Dunin-Borkowski, Y. Mokrousov, S. Blügel, and M. Kläui, Skyrmionic spin structures in layered Fe_5GeTe_2 up to room temperature, Commun. Phys. **5**, 254 (2022).

[14] A. Chakraborty, A. K. Srivastava, A. K. Sharma, A. K. Gopi, K. Mohseni, A. Ernst, H. Deniz, B. K. Hazra, S. Das, P. Sessi, I. Kostanovskiy, T. Ma, H. L. Meyerheim, and S. S. P. Parkin, Magnetic skyrmions in a thickness tunable 2D ferromagnet from a defect driven Dzyaloshinskii–Moriya interaction, Adv. Mater. **34**, 2108637 (2022).

[15] B. W. Casas, Y. Li, A. Moon, Y. Xin, C. McKeever, J. Macy, A. K. Petford-Long, C. M. Phatak, E. J. G. Santos, E. S. Choi, and L. Balicas, Coexistence of merons with skyrmions in the centrosymmetric van der Waals ferromagnet Fe_5GeTe_2, Adv. Mater. **35**, 2212087 (2023).

[16] A. K. Gopi, A. K. Srivastava, A. K. Sharma, A. Chakraborty, S. Das, H. Deniz, A. Ernst, B. K. Hazra, H. L. Meyerheim, and S. S. Parkin, Thickness-tunable zoology of magnetic spin textures observed in Fe_5GeTe_2, ACS Nano **18**, 5335 (2024).

[17] X. Lv, Y. Huang, K. Pei, C. Yang, T. Zhang, W. Li, G. Cao, J. Zhang, Y. Lai, and R. Che, Manipulating the magnetic bubbles and topological Hall effect in 2D magnet Fe_5GeTe_2, Adv. Funct. Mater. **34**, 2308560 (2024).

[18] D. Li, S. Haldar, L. Kollwitz, H. Schrautzer, M. A. Goerzen, and S. Heinze, Prediction of stable nanoscale skyrmions in monolayer Fe_5GeTe_2, Phys. Rev. B **109**, L220404 (2024).

[19] J. Sampaio, A. Pascaud, E. Quero, A. Thiaville, V. Polewczyk, A. Marty, F. Bonell, and A. Mougin, Dzyaloshinskii–Moriya interaction in Fe_5GeTe_2 epitaxial thin films, Nano Lett. **25**, 14341 (2025).

[20] T. T. Ly, J. Park, K. Kim, H.-B. Ahn, N. J. Lee, K. Kim, T.-E. Park, G. Duvjir, N. H. Lam, K. Jang, C.-Y. You, Y. Jo, S. K. Kim, C. Lee, S. Kim, and J. Kim, Direct observation of Fe-Ge ordering in $Fe_{5-x}GeTe_2$ crystals and resultant helimagnetism, Adv. Funct. Mater. **31**, 2009758 (2021).

[21] L. Peng, F. S. Yasin, T.-E. Park, S. J. Kim, X. Zhang, T. Nagai, K. Kimoto, S. Woo, and X. Yu, Tunable Néel–Bloch magnetic twists in Fe_3GeTe_2 with van der Waals structure, Adv. Funct. Mater. **31**, 2103583 (2021).

[22] T.-E. Park, L. Peng, J. Liang, A. Hallal, F. S. Yasin, X. Zhang, K. M. Song, S. J. Kim, K. Kim, M. Weigand, G. Schütz, S. Finizio, J. Raabe, K. Garcia, J. Xia, Y. Zhou, M. Ezawa, X. Liu, J. Chang, H. C. Koo *et al.*, Néel-type skyrmions and their current-induced motion in van der Waals ferromagnet-based heterostructures, Phys. Rev. B **103**, 104410 (2021).

[23] M. Ghidini, V. Farenkov, Y. Li, P. J. Newton, R. Pellicelli, S. Kurdi, N. A. Stelmashenko, F. Maccherozzi, C. H. W. Barnes, A. F. May, M. Chhowalla, S. S. Dhesi, and N. D. Mathur, Inhomogeneous magnetic anisotropy in an $Fe_{5-x}GeTe_2$ nanoflake observed by imaging, ACS Nano **19**, 26193 (2025).

[24] Q. Li, M. Yang, C. Gong, R. V. Chopdekar, A. T. N'Diaye, J. Turner, G. Chen, A. Scholl, P. Shafer, E. Arenholz, A. K. Schmid, S. Wang, K. Liu, N. Gao, A. S. Admasu, S.-W. Cheong, C. Hwang, J. Li, F. Wang, X. Zhang *et al.*, Patterning-induced ferromagnetism of Fe_3GeTe_2 van der Waals materials beyond room temperature, Nano Lett. **18**, 5974 (2018).

[25] L. Rondin, J.-P. Tetienne, T. Hingant, J.-F. Roch, P. Maletinsky, and V. Jacques, Magnetometry with nitrogen-vacancy defects in diamond, Rep. Prog. Phys. **77**, 056503 (2014).

[26] S. Fredericks, K. Parrish, D. Sayre, and Q. Zhu, PyXtal: A python library for crystal structure generation and symmetry analysis, Comput. Phys. Commun. **261**, 107810 (2021).

[27] S. Haastrup, M. Strange, M. Pandey, T. Deilmann, P. S. Schmidt, N. F. Hinsche, M. N. Gjerding, D. Torelli, P. M. Larsen, A. C. Riis-Jensen, J. Gath, K. W. Jacobsen, J. Jørgen Mortensen, T. Olsen, and K. S. Thygesen, The computational 2D materials database: High-throughput modeling and discovery of atomically thin crystals, 2D Mater. **5**, 042002 (2018).

[28] M. N. Gjerding, A. Taghizadeh, A. Rasmussen, S. Ali, F. Bertoldo, T. Deilmann, N. R. Knøsgaard, M. Kruse, A. H. Larsen, S. Manti, T. G. Pedersen, U. Petralanda, T. Skovhus, M. K. Svendsen, J. J. Mortensen, T. Olsen, and K. S. Thygesen, Recent progress of the computational 2D materials database (C2DB), 2D Mater. **8**, 044002 (2021).

[29] See Supplemental Material at http://link.aps.org/supplemental/10.1103/v5zf-5z78 for details about the macroscopic characterization of the sample, about the calibration of the diamond probe, about the extraction of the magnetization from stray field maps and about the magnetic anisotropy used in the simulations, as well as Additional images of disks, together with further micromagnetic simulations, which includes Refs. [50–52].

[30] C. Zhang, Z. Jiang, J. Jiang, W. He, J. Zhang, F. Hu, S. Zhao, D. Yang, Y. Liu, Y. Peng, H. Yang, and H. Yang, Above-room-temperature chiral skyrmion lattice and dzyaloshinskii–moriya interaction in a van der Waals ferromagnet $Fe_{3-x}GaTe_2$, Nat. Commun. **15**, 4472 (2024).

[31] Y. Yuan, D. Liu, J. Yu, G. Zhang, X. Chen, R. Liu, S. Wang, F. Pei, L. Wei, Z. Li, J. Guo, S. Wang, Z. Liao, W. Yan, Z. Qiu, M. Yang, and Q. Li, Modulating above-room-temperature magnetism in Ga-implanted Fe_5GeTe_2 van der Waals magnets, APL Mater. **11**, 091101 (2023).

[32] C. Liu, S. Zhang, H. Hao, H. Algaidi, Y. Ma, and X.-X. Zhang, Magnetic skyrmions above room temperature in a van der Waals ferromagnet Fe_3GaTe_2, Adv. Mater. **36**, 2311022 (2024).

[33] X. Luo, M. Fang, L.-P. Miao, J. Zhao, Z. Shen, W. Fan, X. Ma, Z. Wang, A. Shen, J. Zhang, H. Ye, Y. Xing, X. Yao, F. Ma, N. Zhong, S. Cao, C. Duan, S. Dong, and L. Li, Manipulation of magnetic spin textures at room temperature in a van der Waals ferromagnet, Phys. Rev. B **111**, 014442 (2025).

[34] B. Kim, T. Ochirkhuyag, D. Odkhuu, and S. H. Rhim, Why Fe_3GaTe_2 has higher Curie temperature than Fe_3GeTe_2? arXiv:2504.17998.

[35] A. Finco and V. Jacques, Single spin magnetometry and relaxometry applied to antiferromagnetic materials, APL Mater. **11**, 100901 (2023).

[36] L. Rondin, J.-P. Tetienne, S. Rohart, A. Thiaville, T. Hingant, P. Spinicelli, J.-F. Roch, and V. Jacques, Stray-field imaging of magnetic vortices with a single diamond spin, Nat. Commun. **4**, 2279 (2013).

[37] M. Beg, M. Lang, and H. Fangohr, Ubermag: Towards more effective micromagnetic workflows, IEEE Trans. Magn. **58**, 1 (2022).

[38] M. Donahue and D. Porter, Oommf user's guide, version 2.1a1, https://doi.org/10.18434/T4/1502495, https://math.nist.gov/oommf/software.html.

[39] C. Abert, G. Selke, B. Kruger, and A. Drews, A fast finite-difference method for micromagnetics using the magnetic scalar potential, IEEE Trans. Magn. **48**, 1105 (2012).

[40] T. Shinjo, T. Okuno, R. Hassdorf, K. Shigeto, and T. Ono, Magnetic vortex core observation in circular dots of permalloy, Science **289**, 930 (2000).

[41] J.-P. Tetienne, T. Hingant, L. Rondin, S. Rohart, A. Thiaville, J.-F. Roch, and V. Jacques, Quantitative stray field imaging of a magnetic vortex core, Phys. Rev. B **88**, 214408 (2013).

[42] R. P. Cowburn, D. K. Koltsov, A. O. Adeyeye, M. E. Welland, and D. M. Tricker, Single-Domain circular nanomagnets, Phys. Rev. Lett. **83**, 1042 (1999).

[43] M. Schneider, H. Hoffmann, S. Otto, Th. Haug, and J. Zweck, Stability of magnetic vortices in flat submicron permalloy cylinders, J. Appl. Phys. **92**, 1466 (2002).

[44] K. L. Metlov and K. Y. Guslienko, Stability of magnetic vortex in soft magnetic nano-sized circular cylinder, J. Magn. Magn. Mater. **242-245**, 1015 (2002).

[45] J. Mejía-López, D. Altbir, P. Landeros, J. Escrig, A. H. Romero, I. V. Roshchin, C.-P. Li, M. R. Fitzsimmons, X. Batlle, and I. K. Schuller, Development of vortex state in circular magnetic nanodots: Theory and experiment, Phys. Rev. B **81**, 184417 (2010).

[46] J. C. S. Rocha, P. Z. Coura, S. A. Leonel, R. A. Dias, and B. V. Costa, Diagram for vortex formation in quasi-two-dimensional magnetic dots, J. Appl. Phys. **107**, 053903 (2010).

[47] A. Barman, S. Mondal, S. Sahoo, and A. De, Magnetization dynamics of nanoscale magnetic materials: A perspective, J. Appl. Phys. **128**, 170901 (2020).

[48] G. S. Abo, Y.-K. Hong, J. Park, J. Lee, W. Lee, and B.-C. Choi, Definition of magnetic exchange length, IEEE Trans. Magn. **49**, 4937 (2013).

[49] E. Sfeir, C. Schrader, F. Fabre, J. Courtin, C. Vergnaud, A. Marty, M. Jamet, F. Bonell, I. Robert-Philip, V. Jacques, and A. Finco, Room temperature magnetic vortices in the van der Waals magnet Fe_5GeTe_2 [Dataset], Zenodo (2025), https://doi.org/10.5281/zenodo.15805196.

[50] T. Hingant, J.-P. Tetienne, L. J. Martínez, K. Garcia, D. Ravelosona, J.-F. Roch, and V. Jacques, Measuring the magnetic moment density in patterned ultrathin ferromagnets with submicrometer resolution, Phys. Rev. Appl. **4**, 014003 (2015).

[51] I. Gross, W. Akhtar, V. Garcia, L. J. Martínez, S. Chouaieb, K. Garcia, C. Carrétéro, A. Barthélémy, P. Appel, P. Maletinsky, J.-V. Kim, J. Y. Chauleau, N. Jaouen, M. Viret, M. Bibes, S. Fusil, and V. Jacques, Real-space imaging of non-collinear antiferromagnetic order with a single-spin magnetometer, Nature (London) **549**, 252 (2017).

[52] F. Fabre, A. Finco, A. Purbawati, A. Hadj-Azzem, N. Rougemaille, J. Coraux, I. Philip, and V. Jacques, Characterization of room-temperature in-plane magnetization in thin flakes of $CrTe_2$ with a single-spin magnetometer, Phys. Rev. Mater. **5**, 034008 (2021).